On the post-buckling of distributed microstructured system: The finite element elastica

Article *in* International Journal of Mechanical Sciences · May 2016

DOI: 10.1016/j.ijmecsci.2016.05.009

2 authors:

Attila Kocsis
Robert Bosch Kft., Budapest, Hungary
16 PUBLICATIONS **58** CITATIONS

SEE PROFILE

Noël Challamel
Université de Bretagne Sud
151 PUBLICATIONS **1,361** CITATIONS

SEE PROFILE

International Journal of Mechanical Sciences 114 (2016) 12–20

Contents lists available at ScienceDirect

International Journal of Mechanical Sciences

journal homepage: www.elsevier.com/locate/ijmecsci

On the post-buckling of distributed microstructured system: The finite element *elastica*

Attila Kocsis [a], Noël Challamel [b,*]

[a] Engineering Center Budapest, Robert Bosch Kft., and Department of Structural Mechanics, Budapest University of Technology and Economics, Budapest 1103, Hungary

[b] Université de Bretagne Sud, EA 4250, Institut de Recherche Dupuy de Lôme (IRDL), Centre de Recherche, Rue de Saint Maudé-BP 92116, F-56100 Lorient, France

ARTICLE INFO

Article history:
Received 25 February 2016
Received in revised form
8 May 2016
Accepted 11 May 2016
Available online 12 May 2016

Keywords:
Elastica
Post-buckling
Lattice model
Geometrical nonlinearity
Discrete model
Finite element method
Gradient elasticity
Distributed microstructure

ABSTRACT

The buckling and post-buckling behavior of a simply supported lattice column with distributed microstructure is theoretically and numerically investigated. This problem differs from the nonlinear behavior of a lattice column composed of concentrated microstructure, as illustrated by the Hencky-bar chain system. It is shown that the problem based on a distributed microstructure is mathematically equivalent to the Finite Element formulation of the continuous *elastica* with linear rotation interpolation functions. The buckling load of this lattice column with distributed microstructure is analytically obtained by solving a linear difference boundary value problem. This linearized difference boundary value problem is asymptotically approximated by a continuum gradient elasticity boundary value problem with definite positive equivalent energy functional. The geometrically exact nonlinear behavior of this microstructured column with distributed microstructure is governed by a strongly nonlinear difference equation, which has not been reported in the literature to the authors' knowledge. Bifurcation diagrams of the microstructured column composed of few cells are numerically obtained with the simplex algorithm. It is shown that the post-buckling of the lattice column with distributed microstructure reveals complex behavior similarly to the post-buckling of a lattice column with concentrated microstructure. The first post-buckling branch of the lattice system is compared to that of the gradient *elastica* problem and good correlations are found. The paper is concluded by a general analysis on the effect of concentrated and distributed microstructures at the macroscopic structural scale: Hencky-bar chain system composed of concentrated microstructure asymptotically behaves as a nonlocal (stress gradient) elastic column, whereas the lattice column composed of distributed microstructure asymptotically behaves as a gradient elasticity (strain gradient) elastic column.

1. Introduction

There are numerous works on Finite Element modeling of the *elastica* or geometrically nonlinear elastic structures (see for instance [29,26,24,14,19] – see also the more recent books of [15,30,8,1,21]). These works were essentially devoted to the computation of the geometrically exact post-buckling behavior of the primary branches. The computation of the numerous branches of the bifurcation diagram has not been studied systematically. However, to our knowledge, up to now, results issued for the Finite Element modeling of the planar *elastica* has not revealed the complex nature of the bifurcation diagram, that had been well studied in the past for the finite difference method (or the equivalent Hencky's structural system). In fact, it was shown at the end of the 80's that the post-buckling behavior of the discrete *elastica* problem had a very rich nature inherent to the discrete property of the structural system, with possible spatial chaotic behavior far away from the first post-buckling branch (see for instance [12,10,11,16]). This very rich structure is inherent to the discretization process, which is based on an equivalent finite difference method. This discrete problem referred to as the discrete *elastica* (which can be also classified as a kind of microstructured system with concentrated microstructure) has been recently revisited, using nonlocal elasticity or higher-order gradient elasticity models [5,6]. In fact, there is a strict mathematical correspondence between the lattice column equations with concentrated microstructure (called Hencky-bar system) and the finite difference formulation of the continuous column. The same mathematical equivalence may be found between lattice columns with

* Corresponding author.
E-mail addresses: kocsis@ep-mech.me.bme.hu (A. Kocsis), noel.challamel@univ-ubs.fr (N. Challamel).

http://dx.doi.org/10.1016/j.ijmecsci.2016.05.009
0020-7403/

distributed microstructure and the Finite Element formulation of the continuous column [4]. Therefore, the present study concerns the numerical properties of the Finite Element model and its inherent ability for capturing higher-order branches of the *elastica* problem, and also the post-buckling behavior of lattice columns with distributed microstructure.

Distributed microstructure models have been already considered by Mindlin [22], and recently investigated again by Polyzos et al. [25] or Challamel et al. [7] in the dynamics case. Challamel et al. [7] showed that distributed microstructure models could be handled by equivalent continuous models based on strain gradient elasticity, whereas concentrated microstructure models could be associated with stress gradient elasticity also classified as nonlocal elasticity models. The link between Finite Element modeling, gradient elasticity and models based on distributed microstructure has been outlined for the axial vibrations of bars (equivalent to the torsional or the string problem) by Challamel et al. [7]. The present paper generalizes such kind of results for a beam stability problem in the linear and in the nonlinear ranges. It is worth mentioning that Kocsis [18] already presented buckling results for a micro-structured shear-bending column (a discrete Cosserat rod) with distributed microstructure. As the present paper is also concerned by the possible link between gradient elasticity and micro-structured systems, the paper of Carcaterra et al. [3] can be also mentioned, where higher-order gradient elasticity contributions are shown to be related to long range interaction of the subscale lattice. Dell'Isola et al. [9] generalized Hencky-type discrete systems with both bending and axial interactions.

In this paper we explore a geometrically exact discrete *elastica* with distributed microstructure, i.e. a strongly nonlinear discrete elastic system capable to possess complex bifurcation diagrams. Applications of the paper concern the understanding of micro-structured structural systems in the nonlinear range, as well as the numerical characterization of the Finite Element discretization in presence of strong geometrical nonlinear effects. The nonlinear difference equations of the finite element *elastica* are derived and numerically solved for the simply supported boundary conditions.

2. Finite element *elastica*: a distributed microstructured column

2.1. Governing equations

Let us start with the weak form of the equilibrium equation of a *Bernoulli-Euler* beam under axial compression expressed via the principle of virtual work:

$$\int_0^L EI\theta'\delta\theta' - P\sin\theta\,\delta\theta\;\; ds = 0 \tag{1}$$

Here EI is the bending stiffness of the beam, L is the total length, θ is the rotation of the cross-section as the function of the arc-length parameter s, $\delta\theta$ is a virtual rotation and prime denotes differentiation with respect to s.

We assume a linear interpolation for the rotation field:

$$\theta(\xi) = \theta_{i-1}(1-\xi) + \theta_i\xi \tag{2}$$

Here $\xi = s/a$ is the non-dimensional arc-length parameter, a is the size of the mesh cell, and the notation θ_i is used for the discrete rotation field. The principle of virtual work can be rewritten by summing elementary integral segments on n finite elements:

$$\sum_{i=1}^{n}\int_0^1 \frac{EI}{a^2}\frac{d\theta}{d\xi}\delta\frac{d\theta}{d\xi} - P\sin\theta\,\delta\theta\;\; d\xi = 0 \tag{3}$$

Casting the rotation field in this integral equation leads to the nonlinear difference equation:

$$EI\frac{\theta_{i+1}-2\theta_i+\theta_{i-1}}{a^2} + P\int_0^1 \xi\;\sin\left[\xi(\theta_i-\theta_{i-1})+\theta_{i-1}\right]d\xi + P\int_0^1 (1-\xi)\sin\left[\xi(\theta_{i+1}-\theta_i)+\theta_i\right]d\xi = 0 \tag{4}$$

which can be presented in a single format:

$$EI\frac{\theta_{i+1}-2\theta_i+\theta_{i-1}}{a^2} + P\left(\frac{\cos\theta_i}{\theta_{i+1}-\theta_i} - \frac{\cos\theta_i}{\theta_i-\theta_{i-1}} + \frac{\sin\theta_i-\sin\theta_{i-1}}{(\theta_i-\theta_{i-1})^2} - \frac{\sin\theta_{i+1}-\sin\theta_i}{(\theta_{i+1}-\theta_i)^2}\right) = 0 \tag{5}$$

Eq. (5) is the nonlinear difference equation associated with the finite element *elastica*. By introducing the non-dimensional load parameter $\beta = PL^2/EI$ with $L = n\times a$, Eq. (5) may be expressed as:

$$\theta_{i+1}-2\theta_i+\theta_{i-1} + \frac{\beta}{n^2}\left(\frac{\cos\theta_i}{\theta_{i+1}-\theta_i} - \frac{\cos\theta_i}{\theta_i-\theta_{i-1}} + \frac{\sin\theta_i-\sin\theta_{i-1}}{(\theta_i-\theta_{i-1})^2} - \frac{\sin\theta_{i+1}-\sin\theta_i}{(\theta_{i+1}-\theta_i)^2}\right) = 0 \tag{6}$$

Surprisingly, this nonlinear difference equation is not available in the literature, to the authors' knowledge. It differs from the discrete *elastica* considered by [5,6] using the finite difference method (or equivalently, based on Hencky-based system–see also [2]):

$$EI\frac{\theta_{i+1}-2\theta_i+\theta_{i-1}}{a^2} + P\;\sin(\theta_i) = 0 \tag{7}$$

Sogo [28] used an alternative scheme, also based on energy considerations, and developed:

$$4EI\frac{\sin\left(\frac{\theta_{i+1}-\theta_i}{2}\right) - \sin\left(\frac{\theta_i-\theta_{i-1}}{2}\right)}{a^2} + P\left[\sin\left(\frac{\theta_i+\theta_{i-1}}{2}\right) + \sin\left(\frac{\theta_i+\theta_{i+1}}{2}\right)\right] = 0 \tag{8}$$

which can be also written as:

$$4\frac{EI}{a^2}\;\sin\left(\frac{\theta_{i+1}-2\theta_i+\theta_{i-1}}{4}\right) + P\;\sin\left(\frac{\theta_{i-1}+2\theta_i+\theta_{i+1}}{4}\right) = 0 \tag{9}$$

2.2. Critical loads of the FE elastica

Geometric nonlinearities are fully taken into account in the governing equations of the finite element *elastica*, Eq. (6). If only the proximity of the trivial state is of interest, i.e. the buckling of the column under simple compression, then Eq. (6) can be linearized. First we expand the nonlinear terms as:

$$\frac{\sin\theta_i-\sin\theta_{i-1}}{(\theta_i-\theta_{i-1})^2} - \frac{\cos\theta_i}{\theta_i-\theta_{i-1}} \approx \frac{1-\frac{1}{6}\left(\theta_i^2+\theta_i\theta_{i-1}+\theta_{i-1}^2\right)-1+\frac{\theta_i^2}{2}}{\theta_i-\theta_{i-1}} = \frac{\theta_i}{3}+\frac{\theta_{i-1}}{6} \tag{10a}$$

$$\frac{\sin\theta_i-\sin\theta_{i+1}}{(\theta_i-\theta_{i+1})^2} - \frac{\cos\theta_i}{\theta_i-\theta_{i+1}} \approx \frac{1-\frac{1}{6}\left(\theta_i^2+\theta_i\theta_{i+1}+\theta_{i+1}^2\right)-1+\frac{\theta_i^2}{2}}{\theta_i-\theta_{i+1}} = \frac{\theta_i}{3}+\frac{\theta_{i+1}}{6} \tag{10b}$$

Casting the above formulae in Eq. (6) yields the linear difference equation:

$$\theta_{i+1} - 2\theta_i + \theta_{i-1} + \beta\frac{\theta_{i+1} + 4\theta_i + \theta_{i-1}}{6n^2} = 0 \tag{11}$$

This result is consistent with the literature, but other interpolation fields may also be chosen, as investigated for instance by Seide [27] or Challamel [4].

The boundary conditions of the simply supported column express that the curvature computed from the linear interpolation field vanishes at the ends:

$$\theta_1 = \theta_0 \text{ and } \theta_{n+1} = \theta_n \tag{12}$$

As shown previously by [4], the solution of the linear difference equation system Eq. (11) can be written as

$$\theta_i = A\ \cos(\varphi\, i) + B\ \sin(\varphi\, i) \text{ with } \varphi = \arccos\left(\frac{1 - \frac{\beta}{3n^2}}{1 + \frac{\beta}{6n^2}}\right) \tag{13}$$

Taking into account the boundary conditions, Eq. (12), the above solution leads to the non-dimensional buckling load associated with the k^{th} mode (given by $\sin(\varphi n) = 0$):

$$\beta_{crit,k} = 6n^2\frac{1 - \cos\frac{k\pi}{n}}{2 + \cos\frac{k\pi}{n}} = (k\pi)^2\left[1 + \frac{(k\pi)^2}{12n^2}\right] + o\left(\frac{1}{n^4}\right) \tag{14}$$

Note that the above formula is valid for $n > 2$. The buckling load for the case of $n=2$ will be developed in Section 3.

In the nonlinear range, insertion of the boundary conditions Eq. (12) in the nonlinear difference equation Eq. (5) leads to singularity. Therefore, an asymptotic expansion is needed for $i=1$ and $i=n$ in Eq. (5).

For $i=1$, the nonlinear difference equation Eq. (5) is:

$$EI\frac{\theta_2 - 2\theta_1 + \theta_0}{a^2} + P\left(\frac{\cos\theta_1}{\theta_2 - \theta_1} - \frac{\cos\theta_1}{\theta_1 - \theta_0} + \frac{\sin\theta_1 - \sin\theta_0}{(\theta_1 - \theta_0)^2} - \frac{\sin\theta_2 - \sin\theta_1}{(\theta_2 - \theta_1)^2}\right) = 0 \tag{15}$$

The limit of this difference equation as $\varepsilon = \theta_1 - \theta_0 \to 0$ is:

$$EI\frac{\theta_2 - \theta_1}{a^2} + P\left(\frac{\sin\theta_1}{2} + \frac{\cos\theta_1}{\theta_2 - \theta_1} - \frac{\sin\theta_2 - \sin\theta_1}{(\theta_2 - \theta_1)^2}\right) = 0 \tag{16}$$

due to the asymptotic property

$$-\frac{\cos\theta_1}{\theta_1 - \theta_0} + \frac{\sin\theta_1 - \sin\theta_0}{(\theta_1 - \theta_0)^2} = -\frac{\cos\theta_1}{\varepsilon} + \frac{\sin\theta_1 - \sin(\theta_1 - \varepsilon)}{\varepsilon^2} \underset{\varepsilon\to 0}{\to} \frac{\sin\theta_1}{2} \tag{17}$$

Then, the nonlinear difference equation Eq. (5) for $i=n$, following the same reasoning, yields:

$$EI\frac{-\theta_n + \theta_{n-1}}{a^2} + P\left(\frac{\sin\theta_n}{2} - \frac{\cos\theta_n}{\theta_n - \theta_{n-1}} + \frac{\sin\theta_n - \sin\theta_{n-1}}{(\theta_n - \theta_{n-1})^2}\right) = 0 \tag{18}$$

Finally, the nonlinear difference equation system of the FEM *elastica* (or lattice column with distributed microstructure) can be written in a non-dimensional form:

$$\theta_2 - \theta_1 + \frac{\beta}{n^2}\left(\frac{\sin\theta_1}{2} + \frac{\cos\theta_1}{\theta_2 - \theta_1} - \frac{\sin\theta_2 - \sin\theta_1}{(\theta_2 - \theta_1)^2}\right) = 0 \tag{19a}$$

$$\theta_{i+1} - 2\theta_i + \theta_{i-1} + \frac{\beta}{n^2}\left(\frac{\cos\theta_i}{\theta_{i+1} - \theta_i} - \frac{\cos\theta_i}{\theta_i - \theta_{i-1}} + \frac{\sin\theta_i - \sin\theta_{i-1}}{(\theta_i - \theta_{i-1})^2} - \frac{\sin\theta_{i+1} - \sin\theta_i}{(\theta_{i+1} - \theta_i)^2}\right) = 0 \tag{19b}$$

for $i = 2, \ldots, n-1$, and

$$-\theta_n + \theta_{n-1} + \frac{\beta}{n^2}\left(\frac{\sin\theta_n}{2} - \frac{\cos\theta_n}{\theta_n - \theta_{n-1}} + \frac{\sin\theta_n - \sin\theta_{n-1}}{(\theta_n - \theta_{n-1})^2}\right) = 0 \tag{19c}$$

The boundary conditions are already taken into account in this formalism. Some symmetrical properties are investigated for the studied discrete system in the next section.

2.3. Symmetries in the equilibrium states of the FE elastica

Let us denote a solution of Eq. (19) (i.e., an equilibrium configuration) by $\underline{\theta}^{eq} = \{\theta_1^{eq}, \theta_2^{eq}, \ldots, \theta_n^{eq}\}$ and β^{eq}. It can be shown that another solution can be obtained either by

$$A)\ \underline{\theta} = -\underline{\theta}^{eq} \text{ and } \beta = \beta^{eq} \tag{20a}$$

or by

$$B)\ \theta_i = \theta_i^{eq} + j\pi \text{ and } \beta = (-1)^j\beta^{eq},\ i = 1, \ldots, n,\ j = 1, 2, \ldots \tag{20b}$$

The solutions can be represented uniquely in the $n+1$ dimensional space $(\underline{\theta}, \beta)$, called the Global Representation Space (GRS). In this space symmetry *A)* is a point symmetry in the $\underline{\theta}$ subspace and *B)* is a shift symmetry in the $\underline{\theta}$ subspace. In terms of the geometry of the equilibrium configuration symmetry *A)* means that the mirror image of an equilibrium configuration to the line of action of the load is also an equilibrium configuration, while symmetry *B)* means that rotating an equilibrium configuration about one end by an angle $j\pi$ is also an equilibrium configuration. Note that the consecutive application of *A)* and *B)* yields the solution $\theta_i = -\theta_i^{eq} + j\pi$ and $\beta = (-1)^j\beta^{eq}$.

3. Analytical solution of the nonlinear difference equation–case $n=2$

Analytical solution of the post-bifurcation branches can be obtained in the case of $n=2$. Using Eq. (19), the case of $n=2$ is fully characterized by the set of nonlinear equations:

$$\theta_2 - \theta_1 + \frac{\beta}{4}\left(\frac{\sin\theta_1}{2} + \frac{\cos\theta_1}{\theta_2 - \theta_1} - \frac{\sin\theta_2 - \sin\theta_1}{(\theta_2 - \theta_1)^2}\right) = 0 \tag{21a}$$

$$-\theta_2 + \theta_1 + \frac{\beta}{4}\left(\frac{\sin\theta_2}{2} - \frac{\cos\theta_2}{\theta_2 - \theta_1} + \frac{\sin\theta_2 - \sin\theta_1}{(\theta_2 - \theta_1)^2}\right) = 0 \tag{21b}$$

Summing the above equations yields $\beta = 0$ (unloaded state) or

$$\frac{\sin\theta_1 + \sin\theta_2}{2} + \frac{\cos\theta_1 - \cos\theta_2}{\theta_2 - \theta_1} = \sin\left(\frac{\theta_1 + \theta_2}{2}\right)\cos\left(\frac{\theta_1 - \theta_2}{2}\right) - 2\frac{\sin\left(\frac{\theta_1+\theta_2}{2}\right)\sin\left(\frac{\theta_1-\theta_2}{2}\right)}{\theta_2 - \theta_1} = 0$$

Hence, either

$$\sin\left(\frac{\theta_1 + \theta_2}{2}\right) = 0 \tag{22}$$

or

$$\frac{\theta_2 - \theta_1}{2} + \tan\left(\frac{\theta_2 - \theta_1}{2}\right) = 0 \tag{23}$$

Eq. (22) yields $\theta_1+\theta_2+2(k-1)\pi=0$, which leads to the following equilibrium paths:

$$\theta_1+(k-1)\pi-\frac{\beta}{16}\left(\sin\theta_1-\frac{\cos\theta_1}{\theta_1+(k-1)\pi}+\frac{\sin\theta_1}{\left(\theta_1+(k-1)\pi\right)^2}\right)=0 \tag{24}$$

For $k=1$ the post-buckling (or secondary) equilibrium path is obtained:

$$\theta_1-\frac{\beta}{16}\left(\sin\theta_1-\frac{\cos\theta_1}{\theta_1}+\frac{\sin\theta_1}{{\theta_1}^2}\right)=0 \tag{25}$$

Eq. (23) can only be solved numerically for $(\theta_2-\theta_1)/2$. The roots are denoted by $-b_m$. Hence, $\theta_2-\theta_1+2b_m=0$, which leads to the following equilibrium paths:

$$b_m-\frac{\beta}{16}\left(\sin\theta_1-\frac{\cos\theta_1}{b_m}+\frac{\sin\theta_1}{2{b_m}^2}-\frac{\sin(\theta_1-2b_m)}{2{b_m}^2}\right)=0 \tag{26}$$

The first five solutions for b_m are obtained numerically and given in Table 1. Note that $b_{-m}=-b_m$.

Fig. 1 shows the equilibrium paths of the FEM elastica with $n=2$ element, based on the above analytical solutions.

Now, having derived the exact analytical solution for $n=2$, the buckling load can be developed. The Taylor expansion of the post-buckling path, Eq. (25), up to the first-order of θ_1 is:

$$\theta_1-\frac{\beta}{16}\left(\theta_1-\frac{1-\theta_1^2/2}{\theta_1}+\frac{\theta_1-\theta_1^3/6}{{\theta_1}^2}\right)=\theta_1-\frac{\beta}{16}\left(\frac{16}{12}\theta_1\right)=0$$

By using the equilibrium method for computing critical forces [17], the first variation of the above equation leads to the critical (buckling) load parameter of the FEM elastica of $n=2$ cells:

$$\beta_{crit}=12 \tag{27}$$

This value is confirmed by the bifurcation diagrams and also by the forthcoming numerical results.

For completeness we note that the *Hencky* chain of $n=2$ links has also two sets of solutions, both of which can be obtained analytically. The first set is:

$$\theta_1+(k-1)\pi-\frac{\beta}{8}\sin(\theta_1)=0 \tag{28}$$

which yields the secondary (or post-buckling) equilibrium path for $k=1$:

$$\theta_1-\frac{\beta}{8}\sin(\theta_1)=0 \tag{29}$$

The other set of solutions of *Hencky*'s system of $n=2$ links is:

$$(2l+1)\pi-\frac{\beta}{4}\sin(\theta_1)=0 \tag{30}$$

Fig. 2 shows the equilibrium paths (bifurcation diagram) of the *Hencky* chain of $n=2$ links. Fig. 3 compares the post-buckling path of the FEM elastica of $n=2$ elements (black) and that of the *Hencky* chain of $n=2$ links (gray). Dotted line indicates π^2, the non-dimensional buckling load of the elastica. Here it can be seen that the FEM elastica is stiffer, while the *Hencky* chain is softer than their corresponding continuum model, the *elastica*. Fig. 4 compares the equilibrium paths of the FEM elastica and the Hencky chain for $n=2$ cells.

Note that due to symmetries *A)* and *B)* it would be sufficient to show the bifurcation diagram in $\theta_1\in[0,\pi)$ and $\beta\geq 0$.

Table 1
First five solutions of Eq. (23) for b_m with $b_m=-(\theta_2-\theta_1)/2$.

m	1	2	3	4	5
b_m	2.02876	4.91318	7.72525	11.08554	14.20744

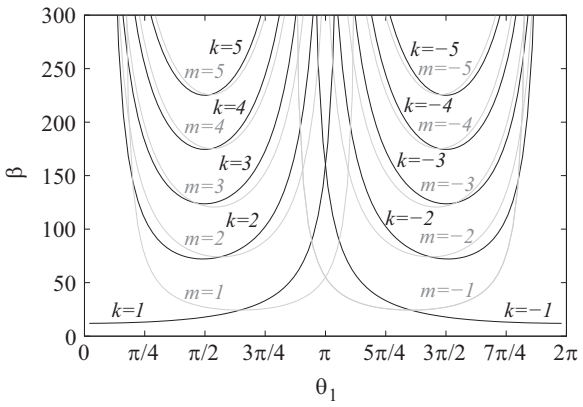

Fig. 1. Equilibrium paths of the FEM *elastica* for $n=2$. Black paths are associated with Eq. (24) and gray paths are originated from Eq. (26).

4. Numerical solutions

Analytical solutions for $n>2$ cells are not available. Instead, numerical simulations can be applied for approximating the equilibrium states of the FE elastica. However, the numerical procedure applicable for *Hencky*'s system [12] cannot be used here. The algorithm for Hencky's system was based on rewriting Eq. (7) in the following map:

$$\kappa_{i+1}=\kappa_i-\frac{\beta}{n^2}\sin(\theta_i),$$

$$\theta_{i+1}=\theta_i+\kappa_{i+1},$$

$i=1,\cdots,n$. In fact, the above map is equivalent to the standard map, a well-know chaotic, area preserving map [11]. Starting with the boundary condition $\kappa_1=0$, and choosing an appropriate value for the initial angle θ_1, the above map can be iterated, κ_{n+1} can be computed, and it can be checked if the far-end boundary condition ($\kappa_{n+1}=0$) fulfils or not. The shooting technique then can be applied: by slightly varying the initial angle and checking if κ_{n+1} changes sign allows us to find approximate solutions for fixed load levels. Thus, each solution of the *Hencky* problem *can be represented uniquely* in a 3D space spanned by $(\theta_1,\kappa_1,\beta)$. See Gáspár and Domokos [12], Kocsis and Károlyi [16], or Kocsis [17] for more details.

In the present case, however, Eq. (19b) can be rewritten as:

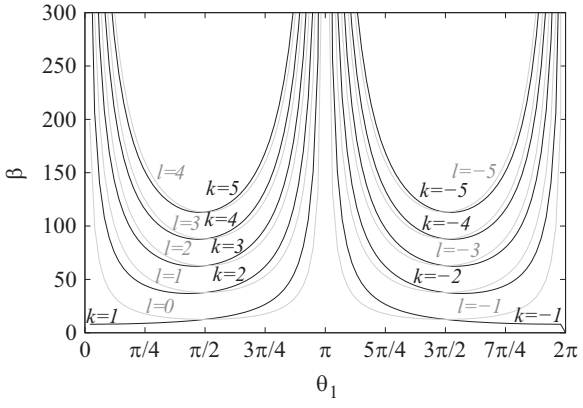

Fig. 2. Equilibrium paths of the *Hencky* chain for $n=2$. Black paths are associated with Eq. (28) and gray paths are originated from Eq. (30).

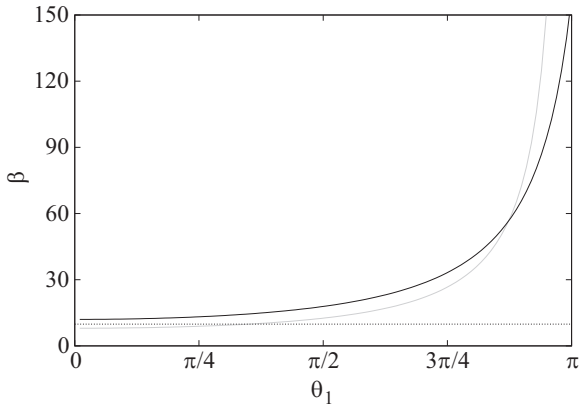

Fig. 3. Secondary path of the FEM *elastica* (black) and that of the *Hencky* chain (gray) for $n=2$. Dotted line shows the non-dimensional buckling load of the elastica, π^2.

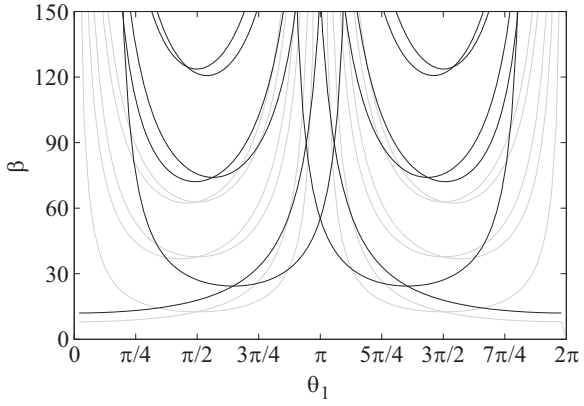

Fig. 4. Equilibrium paths of the FEM *elastica* (black) and of the *Hencky* chain (gray) for $n=2$.

$$\kappa_{i+1} = \kappa_i - \frac{\beta}{n^2}\left(\frac{\cos\theta_i}{\kappa_{i+1}} - \frac{\cos\theta_i}{\kappa_i} + \frac{\sin\theta_i - \sin(\theta_i - \kappa_i)}{\kappa_i^2} - \frac{\sin(\theta_i + \kappa_{i+1}) - \sin\theta_i}{\kappa_{i+1}^2}\right),$$

$$\theta_{i+1} = \theta_i + \kappa_{i+1},$$

$i = 2, \cdots, n-1$. Now the first equation is non linear in κ_{i+1} and hence uniqueness of the solution does not apply. Therefore, the solutions of our problem, the buckling and post-buckling of the FE elastica, *cannot be represented uniquely* in the 3D space $(\theta_1, \kappa_1, \beta)$. Therefore, the previously described shooting technique cannot be applied in this case. Instead, the simplex algorithm is utilized. It is shortly reviewed in the next section.

4.1. The applied numerical algorithm

For larger values of n, the numerical solution for Eq (19) is obtained with the simplex algorithm [13]. The Global Representation Space (GRS), spanned by $(\theta_1, \theta_2, \cdots, \theta_n, \beta)$, is an $n+1$ dimensional space in which the solutions for Eq. (19) are uniquely embedded. Since Eq. (19) defines n equations, the solutions are equilibrium paths. The advantage of the simplex algorithm is that it is capable to approximate all the equilibrium paths (i.e., all the solutions of the nonlinear difference equation system Eq. (19)) without iterations in a bounded domain of the GRS. The algorithm divides the bounded domain of the GRS into hypercubes with a given resolution, then subdivides each hypercube into $(n+1)!$ simplices and solves the equation system with piecewise linearization over each simplex. The drawback of the simplex algorithm is that the computational time increases *exponentially* with the dimension of the GRS. In fact, the number of computational steps is proportional to $D \times n^3 \times (n+1)!$ with D being the number of hypercubes. Therefore, numerical simulations can be accomplished within a reasonable time only for smaller values of n. Since a fairly coarse resolution of the GRS is applied in our analysis, the obtained results are refined with a *Newton-Raphson* iteration. The numerical procedures were developed in FORTRAN 90.

First we verify the code by computing the equilibrium branches for $n=2$ and comparing the result with the analytical solution. Then numerically computed bifurcation diagrams are shown for $n=3$ and $n=4$. We note that obtaining the results for $n=2$ (with GRS resolution discussed in the next section) takes only a few seconds, while for $n=3$ it scales with approximately 10^4 and hence takes about 15 h. If the same resolution is kept the computational time for $n=4$ again scales with around 10^4 and hence it would take 17 years, and for $n=5$ it also scales with about 10^4. These run times correspond to one core of an Intel Core i7-3770 CPU. Even with parallelization on eight cores, the results for $n=4$ are not feasible to obtain only if the resolution of the GRS is decreased. By using a coarser resolution of the GRS for $n=4$ (detailed in the next section) and parallelizing, it took 14 weeks for the simulation to finish. It explains why we do not show numerical results for larger values of the element number n.

4.2. Detailed numerical results, bifurcation diagrams

Fig. 5 shows the numerical solutions of Eq. (19) for $n=2$, i.e. the equilibrium paths of the finite element elastica with $n=2$ cells. The scanned domain of the GRS was $\theta_1 \in [0, \pi]$, $\theta_2 \in [-8\pi, 8\pi]$ and $\beta \in [0, 300]$, discretized in 100x900 × 900 parts. The figure shows the equilibrium paths on $\theta_1 \in [0, 2\pi]$, simply by applying the symmetries *A)* and *B)* (Eq. (20)) on the result of the scanning algorithm. There is one bifurcation on the trivial equilibrium path at $\beta_{crit} = 12$, consistently with Eq. (27).

Note that not all the branches appear in Fig. 5 which are present in Fig. 1. That is because only a finite domain of the GRS was scanned, and the equilibrium paths denoted by $m = k = 5$ and $m = k = -5$ in Fig. 1 are beyond that domain. If the scanned domain is extended to $\theta_2 \in [-10\pi, 10\pi]$, then those missing branches are also found. Thus, it is important to scan a large enough domain of the GRS while keeping the discretization of the space small (i.e., using a fine grid in the GRS). On the other hand, the size of the scanned domain and the resolution of the grid in higher dimensions is limited by the available computational capacities and time.

Eventually, by comparing Fig. 5 to Fig. 1 we can conclude that the same paths are obtained numerically as analytically, which validates our numerical procedure and the code.

Fig. 6 shows the equilibrium paths of the finite element elastica with $n=3$ cells. The scanned domain of the GRS was $\theta_1 \in [0, \pi]$, $\theta_2 \in [-8\pi, 8\pi]$, $\theta_3 \in [-8\pi, 8\pi]$ and $\beta \in [0, 300]$, discretized in $100 \times 900 \times 900 \times 900$ parts. Again, symmetries Eq. (20) were applied to show the equilibrium paths on $\theta_1 \in [0, 2\pi]$.

It can be seen in the figure that there are two equilibrium paths bifurcating from the trivial one. These two pitchfork bifurcations are at the critical load values given by the analytical result Eq. (14): the first is at $\beta_{crit,1} = 54/5 = 10.8$ and the second is at $\beta_{crit,2} = 54$.

Apart from these post-buckling branches, there are many higher-order equilibrium paths, evolving as pitchfork or saddle-node bifurcations.

Fig. 7 shows the equilibrium paths of the finite element elastica with $n=4$ cells. The studied domain of the GRS is $\theta_1 \in [0, \pi]$,

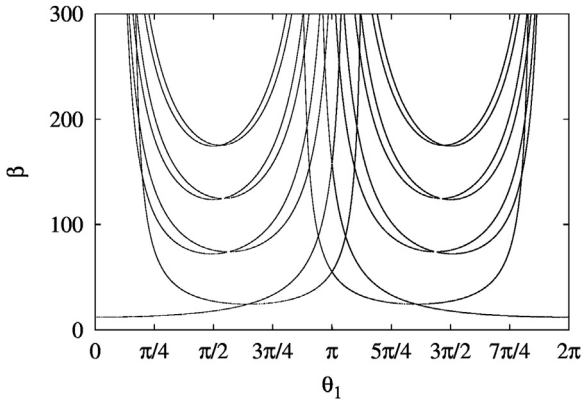

Fig. 5. Equilibrium paths of the FEM *elastica* of $n=2$ cells, computed numerically with the simplex algorithm. The scanned domain was $\theta_1 \in [0, \pi]$, $\theta_2 \in [-8\pi, 8\pi]$ and $\beta \in [0, 300]$.

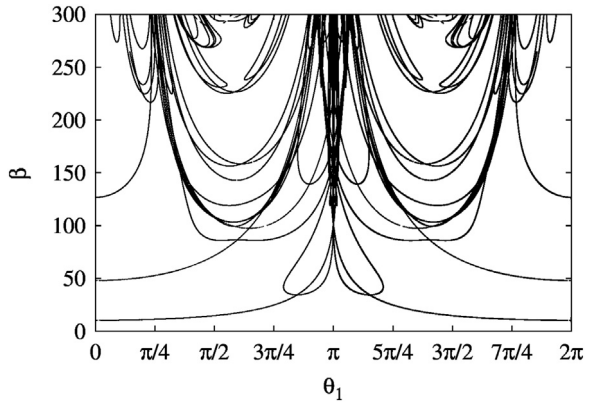

Fig. 7. Equilibrium paths of the FEM *elastica* of $n=4$ cells, computed numerically with the simplex algorithm. The scanned domain was $\theta_1 \in [0, \pi]$, $\theta_2 \in [-8\pi, 8\pi]$, $\theta_3 \in [-8\pi, 8\pi]$, $\theta_4 \in [-8\pi, 8\pi]$ and $\beta \in [0, 300]$.

$\theta_2 \in [-8\pi, 8\pi]$, $\theta_3 \in [-8\pi, 8\pi]$, $\theta_4 \in [-8\pi, 8\pi]$ and $\beta \in [0, 300]$, discretized in $50 \times 800 \times 800 \times 800 \times 300$ parts. Symmetries *A)* and *B)* (Eq. (20)) were applied to show the equilibrium paths on $\theta_1 \in [0, 2\pi]$.

In this case there can be seen three equilibrium paths bifurcating from the trivial one. These pitchfork bifurcations are at the critical load values given analytically by Eq. (14). The first bifurcation is at $\beta_{crit,1} = 10.3866$, the second is at $\beta_{crit,2} = 48$, and the third is at $\beta_{crit,3} = 126.7562$.

There can be seen many pitchfork and saddle-node bifurcations separated from the trivial equilibrium path. Here new, higher-order equilibrium branches appear in great number.

The bifurcation diagram of the finite element *elastica* is similar to that of the *Hencky* chain in the followings: its trivial path has $n-1$ pitchfork bifurcations (here n is the number of cells), it is complex and the number of equilibrium states seems to increase rapidly with the number of cells. It is known that *Hencky*'s system is spatially chaotic [11] and this behavior can be identified by studying the dependence of the number of equilibrium states S on the number of cells n [16]. This dependence is $S \propto \beta^n$, with β being the load parameter, for the spatially chaotic boundary value problem defined by the post-buckling of the *Hencky* chain. To show that spatial chaotic behavior holds for the boundary value problem defined by the post-buckling of the finite element *elastica* would require much more numerical simulations. First, as we saw the size of the scanned domain should be extended to ensure that all equilibrium sates are found. Second, higher load levels should be studied. Lastly, more number of cells should be involved in the analysis. Each of these requirements extremely increases the computational time of the simulations. In this paper we have shown numerical results which were achievable with our available hardware resources. However, based on the similarities of the presented results and bifurcation diagrams to *Hencky*'s system we conjecture that the boundary value problem associated with the post-buckling of the hinged-hinged finite element *elastica* is spatially chaotic.

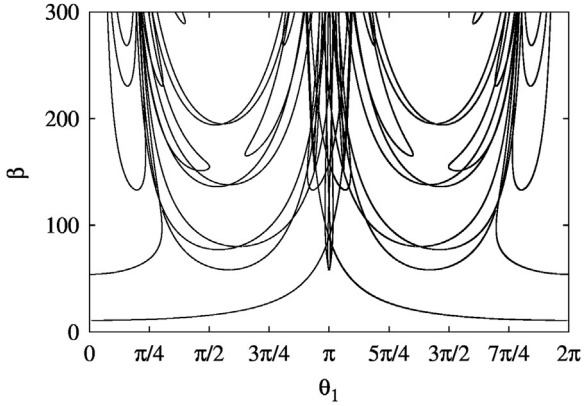

Fig. 6. Equilibrium paths of the FEM *elastica* of $n=3$ cells, computed numerically with the simplex algorithm. The scanned domain was $\theta_1 \in [0, \pi]$, $\theta_2 \in [-8\pi, 8\pi]$, $\theta_3 \in [-8\pi, 8\pi]$ and $\beta \in [0, 300]$.

5. A link with gradient elasticity models

5.1. The gradient elastica: Buckling load

As detailed in [4], a continualization of the linearized second-order difference equation can be written by:

$$EI\left(\theta'' + \frac{a^2}{12}\theta^{(4)} + \ldots\right) + P\left(\theta + \frac{a^2}{6}\theta'' + \ldots\right) = 0 \tag{31}$$

which can be also approximated by:

$$EI\left(\theta'' - \frac{a^2}{12}\theta^{(4)}\right) + P\theta = 0 \tag{32}$$

One recognizes a gradient elasticity model, obtained from the following energy functional:

$$U = \int_0^L \frac{1}{2}EI\theta'^2 + \frac{1}{2}EI\frac{a^2}{12}\theta''^2 - \frac{1}{2}P\theta^2 dx \tag{33}$$

whose Rayleigh quotient is given by:

$$R[\theta] = \frac{EI\int_0^L \theta'^2 + \frac{a^2}{12}\theta''^2 dx}{\int_0^L \theta^2 dx} \geq \frac{EI\int_0^L \theta'^2 dx}{\int_0^L \theta^2 dx} \tag{34}$$

The buckling of finite gradient elasticity columns has been studied by Papargyri-Beskou et al. [23]. Lazopoulos [20] also investigated the post-buckling of long (asymptotically infinite) gradient elasticity columns. For the hinge-hinge column, the buckling load is obtained from (see [23,4]):

$$P_{cr} = \frac{\pi^2 EI}{L^2}\left(1 + \frac{\pi^2 l_c^2}{L^2}\right) \text{ with } l_c^2 = \frac{a^2}{12} \tag{35}$$

which is consistent with the analytical results Eq. (14) issued of the exact microstructured problem.

5.2. The geometrically exact gradient elastica

It is then reasonable to use the gradient *elastica* as a possible

enriched continua for the geometrically exact lattice column with distributed microstructure. The gradient elastica is obtained from the following energy functional:

$$U = \int_0^L \frac{1}{2}EI\theta'^2 + \frac{1}{2}EI\frac{a^2}{12}\theta''^2 - P(1 - \cos\ \theta)ds \tag{36}$$

The stationarity, $\delta U = 0$, of the above functional leads to the differential equation of the gradient *elastica*:

$$EI\left(\theta'' - l_c^2\theta^{(4)}\right) + P\ \sin\ \theta = 0 \text{ with } l_c^2 = \frac{a^2}{12} \tag{37}$$

This nonlinear differential equation is closed to the one investigated by [6], obtained for a higher-order gradient elasticity system with non-definite positive energy functional, associated with a positive sign in front of the fourth-order derivative of the rotation in the governing equation, instead of the negative one considered in this study.

The differential equation Eq. (37) can be numerically solved if four associated boundary conditions are given. The first set of boundary conditions is derived from application of the variational principle $\delta U = 0$, leading to:

$$\left[EI\frac{a^2}{12}\theta''\delta\theta'\right]_0^L + \left[EI\left(\theta' - \frac{a^2}{12}\theta'''\right)\delta\theta\right]_0^L = 0 \tag{38}$$

One recognizes the gradient elasticity beam model, as considered by Lazopoulos [20] or Papargyri-Beskou et al. [23] with positive definite energy. The natural boundary condition in Eq. (38) defines the bending moment as:

$$M = EI\left(\kappa - \frac{a^2}{12}\kappa''\right) \text{ with } \kappa = \theta' \tag{39}$$

The centered boundary conditions of this second-order gradient elasticity model may be chosen from Eq. (38):

$$\theta'(0) = \theta'(L) = 0 \text{ and } \theta'''(0) = \theta'''(L) = 0 \tag{40}$$

As discussed in [5] or [6], the uncentered boundary conditions obtained by continualization of the discrete-based boundary conditions Eq. (12) of this second-order gradient elasticity model are chosen as:

$$\theta'\left(\frac{a}{2}\right) = \theta'\left(L + \frac{a}{2}\right) = 0 \text{ and } \theta'''\left(\frac{a}{2}\right) = \theta'''\left(L + \frac{a}{2}\right) = 0 \tag{41}$$

The nonlinear differential equation of the gradient elastica, Eq. (37), can be non-dimensionalized. Let us introduce the non-dimensional arc-length parameter $\varsigma = s/L$. The rotation field with the non-dimensional arc-length is given by $\hat{\theta}(\varsigma) = \theta(\varsigma \cdot L)$, which implies $\theta'(s) = \frac{d\theta}{ds} = \frac{d\hat{\theta}}{d\varsigma}\frac{1}{L} = d_\varsigma\hat{\theta}\frac{1}{L}$. Here $d_\varsigma = \frac{d}{d\varsigma}$ denotes differentiation with respect to the non-dimensional arc-length parameter ς. Then, let us introduce the non-dimensional load parameter as $\beta = \frac{PL^2}{EI}$. Finally, the non-dimensional differential equation yields:

$$d_\varsigma^4\hat{\theta} - 12n^2\left(d_\varsigma^2\hat{\theta} + \beta\ \sin\ \hat{\theta}\right) = 0 \tag{42}$$

Using *Cauchy*'s reformulation, the fourth-order nonlinear ordinary differential equation, Eq. (42), is rewritten into the following first-order ordinary differential equation system:

$$\begin{aligned} d_\varsigma\hat{\theta} &= \kappa \\ d_\varsigma\kappa &= \gamma \\ d_\varsigma\gamma &= \alpha \\ d_\varsigma\alpha &= 12n^2\left(\gamma + \beta\ \sin\ \hat{\theta}\right) \end{aligned} \tag{43}$$

For this differential equation system, the centered boundary conditions are represented by:

$$\kappa(0) = \kappa(1) = 0 \text{ and } \alpha(0) = \alpha(1) = 0 \tag{44}$$

while the uncentered boundary conditions are:

$$\kappa\left(\frac{1}{2n}\right) = \kappa\left(1 + \frac{1}{2n}\right) = 0 \text{ and } \alpha\left(\frac{1}{2n}\right) = \alpha\left(1 + \frac{1}{2n}\right) = 0 \tag{45}$$

5.3. First post-buckling path, comparison to FE elastica

The differential equation system Eq. (43) can be solved numerically with either the centered or uncentered boundary conditions, Eq. (44) or Eq. (45), respectively. The simplex algorithm [13] is used for following the first post-buckling branch of the gradient elastica and results are compared to the first post-buckling branch of the FE elastica.

Fig. 8 shows the first post-buckling path of the FE elastica (black), the gradient elastica with centered local boundary conditions (dark gray), and the gradient elastica with uncentered nonlocal boundary conditions (light gray) for $n=2$, 3, 4 and 5.

It can be seen that the gradient elasticity model approximates very well the microstructured model, the FE elastica. The secondary paths of the gradient elastica with centered and uncentered boundary conditions enclose the secondary path of the FE elastica. It can be observed that for large displacements the gradient elastica is stiffer with uncentered boundary conditions than with centered boundary conditions.

It is worth noting that the case of $n=2$ is an exception. Here the buckling load formula Eq. (35) (and equivalently Eq. (14)) yields $\beta_{crit}^{grad} = 11.899$ for the gradient elastica, while Eq. (14) is not valid for the FE elastica with $n=2$ cells, instead $\beta_{crit}^{FE} = 12$, according to Eq. (27). Hence, for small displacements the gradient elastica is softer than the FE elastica, but for larger displacements the secondary path of the gradient elastica with centered and uncentered boundary conditions again enclose the secondary path of the FE elastica.

Table 2 shows detailed numerical results for the first post-buckling path of the FE elastica, the gradient elastica with centered local boundary conditions, and the gradient elastica with uncentered nonlocal boundary conditions for $n=4$. Here the good correlation between the post-buckling behaviors of the FE elastica and the gradient elastica with centered and uncentered boundary conditions can be also well observed. To summarize, the effect of concentrated and distributed microstructures can be captured at the macroscopic structural scale: Hencky-bar chain system composed of concentrated microstructure asymptotically behaves as a nonlocal (stress gradient) elastic column (as shown by [5] or [31]), whereas the lattice column composed of distributed microstructure asymptotically behaves as a gradient elasticity (strain gradient) elastic column.

6. Conclusions

The buckling and post-buckling behavior of a lattice column with distributed microstructure has been analytically and numerically investigated. This problem is equivalent to a Finite Element formulation of the discretized *elastica*. Exact solution of the linearized problem has been obtained. The post-buckling of the lattice column with distributed microstructure reveals complex behavior, characterized by a vast number of higher-order branches, sometimes referred to as parasitic solutions, which is a phenomenon already investigated for the post-buckling of the lattice column with concentrated microstructure (as another discrete

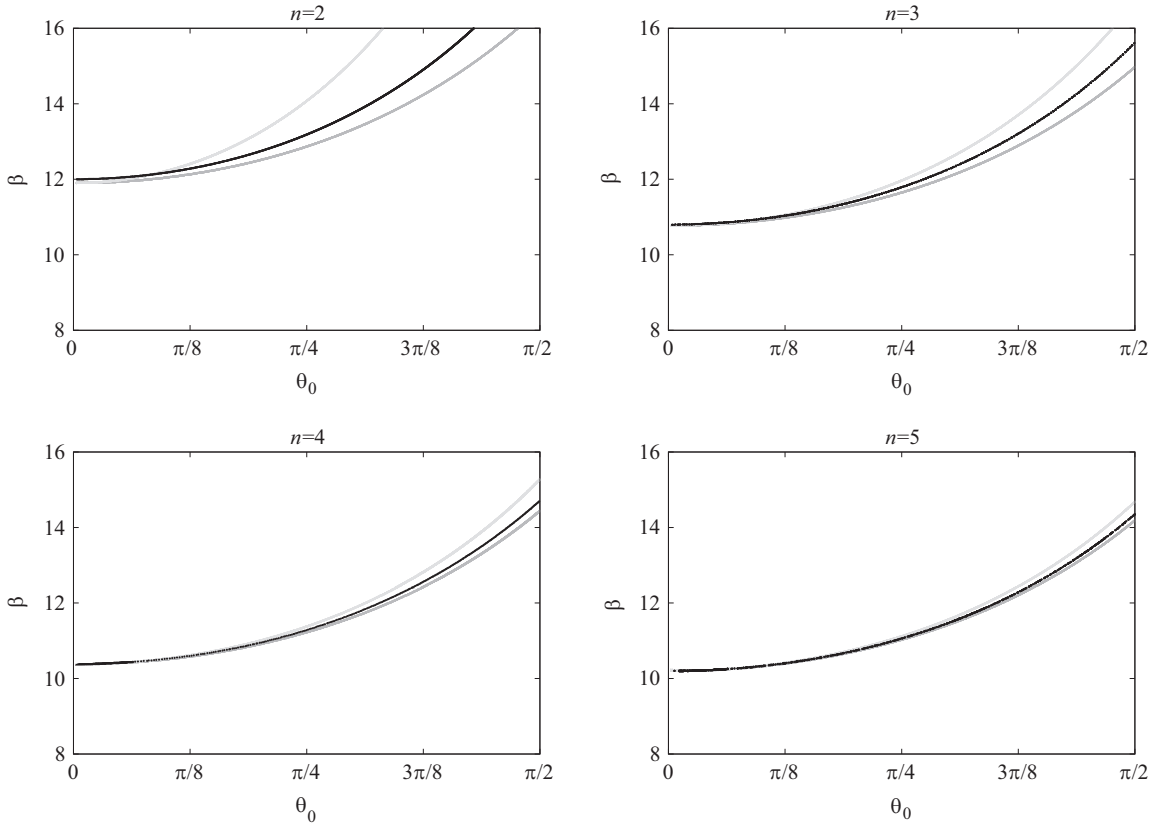

Fig. 8. First post-buckling path of the FE *elastica* (black), the gradient *elastica* with centered local boundary conditions (dark gray), and the gradient *elastica* with uncentered nonlocal boundary conditions (light gray) for $n=2$, 3, 4 and 5. (*Note* that $\theta_0=\theta_1$ for the finite element *elastica*).

Table 2
Computation of first post-buckling branch $\beta=f(\theta_0)$ in the case of $n=4$; centered local boundary conditions are characterized by $\theta'(0)=\theta'(L)=0$ and $\theta'''(0)=\theta'''(L)=0$; uncentred nonlocal boundary conditions are characterized by $\theta'(a/2)=\theta'(L+a/2)=0$ and $\theta'''(a/2)=\theta'''(L+a/2)=0$.

$\theta(0)=\theta_0$	β (discrete system)	β (Gradient elasticity; centered local boundary conditions)	β (Gradient elasticity; uncentred nonlocal boundary conditions)	β (*Elastica* solution)
0	$6n^2\frac{1-\cos\frac{\pi}{n}}{2+\cos\frac{\pi}{n}}$	$\pi^2\left[1+\frac{\pi^2}{12n^2}\right]$	$\pi^2\left[1+\frac{\pi^2}{12n^2}\right]$	$\pi^2\approx 9.8696$
	$=\frac{96}{7}\left(5-3\sqrt{2}\right)$	$=\pi^2\left[1+\frac{\pi^2}{192}\right]$	$=\pi^2\left[1+\frac{\pi^2}{192}\right]$	
	≈ 10.3866	≈ 10.3769	≈ 10.3769	
0.25	10.472	10.458	10.472	9.947
0.5	10.737	10.708	10.766	10.185
0.75	11.201	11.144	11.281	10.600
1	11.895	11.797	12.058	11.222
1.25	12.878	12.719	13.166	12.104
1.5	14.238	13.992	14.719	13.326
1.75	16.119	15.753	16.900	15.023
2	18.764	18.228	20.031	17.430

elastica). The bifurcation diagram has been obtained numerically for some small number of cells, by the application of the simplex algorithm. The results show that the discrete model inherently contains some specific features that continuum models cannot capture. The specific higher-order branches, sometimes classified as parasitic branches, do not appear in the analogous continuous problem.

Numerical results have been corroborated with analytical results for the microstructured column with few periodic cells. The first post-buckling path of the finite element elastica has been compared to that of a gradient elasticity model with positive definite energy functional, using both centered and uncentered boundary conditions for the gradient *elastica*. It has been shown that gradient elasticity is able to capture the buckling as well as post-buckling behavior of lattice structural system with distributed microstructure, at least for the first post-buckling branch. In conclusions, the distribution properties of the microstructure at the micro-scale (concentrated or distributed microstructures) have some strong influence on the macroscopic response at the structural scale: Hencky-bar chain system composed of concentrated microstructure asymptotically behaves as a nonlocal (stress gradient) elastic column, whereas the lattice column composed of distributed microstructure asymptotically behaves, as highlighted in this paper, as a gradient elasticity (strain gradient) elastic column. Some generalization of these results may be obtained with some more general microstructure distribution, or taking into account some more interaction with long range dependence.

Acknowledgment

The work of A. Kocsis was supported by the János Bolyai Research Scholarship of the Hungarian Academy of Sciences.

References

[1] Belytschko T, Liu WK, Moran B, Elkhodary K. Nonlinear finite elements for continua and structures. London: Wiley; 2013.
[2] Bruckstein AM, Holt RJ, Netravali AN. Discrete *elastica*. Appl Anal: Int J 2001;78 (3-4):453–85.

[3] Carcaterra A, dell'Isola F, Esposito R, Pulvirenti M. Macroscopic description of microscopically strongly inhomogenous systems: A mathematical basis for the synthesis of higher gradients metamaterials. Arch Ration Mech Anal 2015;218 (3):1239–62.
[4] Challamel N, Picandet V, Collet B, Michelitsch T, Elishakoff I, Wang CM. Revisiting finite difference and finite element methods applied to structural mechanics within enriched continua. Eur J Mech A/Solids 2015;53:107–20.
[5] Challamel N, Kocsis A, Wang CM. Discrete and nonlocal *elastica*. Int J Nonlinear Mech 2015;77:128–40.
[6] Challamel N, Kocsis A, Wang CM. Higher-order gradient elasticity models applied to geometrically nonlinear discrete systems. Theor Appl Mech 2015;42 (4):223–48.
[7] Challamel N, Wang CM, Elishakoff I. Nonlocal or gradient elasticity macroscopic models: a question of concentrated or distributed microstructure. Mech Res Commun 2016;71:25–31.
[8] De Borst R, Crisfield MA, Remmers JJC, Verhoosel CV. Non-linear finite element analysis of solids and structures. Wiley; 2012.
[9] Dell'Isola F, Giorgio I, Pawlikowski M, Rizzi NL. Large deformations of planar extensible beams and pantographic lattices: Heuristic homogenisation, experimental and numerical examples of equilibrium. Proc R Soc A 2016;472:2185.
[10] Domokos G. Qualitative convergence in the discrete approximation of the Euler problem. Mech Struct Mach 1993;21(4):529–43.
[11] Domokos G, Holmes P. Euler's problem, Euler's method, and the standard map; or, the discrete charm of buckling. J Nonlinear Sci 1993;3:109–51.
[12] Gáspár Z, Domokos G. Global investigation of discrete models of the Euler buckling problem. Acta Tech Acad Sci Hung 1989;102:227–38.
[13] Gáspár Z, Domokos G, Szeberényi I. A parallel algorithm for the global computation of elastic bar structures. CAMES 1997;4:55–68.
[14] Golley BW. The finite element solution of a class of elastica problem. Comput Methods Appl Mech Eng 1984;46(2):159–68.
[15] Hjelmstad KD. Fundamentals of structural mechanics. New York: Springer; 2005.
[16] Kocsis A, Károlyi G. Conservative spatial chaos of buckled elastic linkages. Chaos 2006;16 033111/1-7.
[17] Kocsis A. An equilibrium method for the global computation of critical configurations of elastic linkages. Comput Struct 2013;121:50–63.
[18] Kocsis A. Buckling analysis of the discrete planar cosserat rod. Int J Struct Stab Dyn 2016;16(1):1–29 1450111.
[19] Kondoh K, Atluri SN. A simplified finite element method for large deformation, post-buckling analyses of large frame structures, using explicitly derived tangent stiffness matrices. Int J Numer Methods Eng 1986;23:69–90.
[20] Lazopoulos KA. Post-buckling problems for long elastic beams. Acta Mech 2003;164:189–98.
[21] Luongo A, Zulli D. Mathematical models of beams and cables. London: ISTE-Wiley; 2013.
[22] Mindlin RD. Micro-structure in linear elasticity. Arch Ration Mech Anal 1964;16:51–78.
[23] Papargyri-Beskou S, Tsepoura KG, Polyzos D, Beskos DE. Bending and stability analysis of gradient elastic beams. Int J Solids Struct 2003;40:385–400.
[24] Pignataro M, Di Carlo A, Casciaro R. On nonlinear beam models from the point of view of computational post-buckling analyses. Int J Solids Struct 1982;18 (4):327–47.
[25] Polyzos D, Huber G, Mylonakis G, Triantafyllidis T, Papargyri-Beskou S, Beskos DE. Torsional vibrations of fine-grained material: a gradient elasticity approach. J Mech Phys Solids 2015;76:338–58.
[26] Schmidt WF. Finite element solution for the *elastica*. J Eng Mech 1977;103 (6):1171–5.
[27] Seide P. Accuracy of some numerical methods for column buckling. J Eng Mech 1975;101(5):549–60.
[28] Sogo K. Variational discretization of Euler's *elastica* problem. J Phys Soc Jpn 2006;75:064007.
[29] Tada Y, Lee GC. Finite element solution to an *elastica* problem of beams. Int J Numer Methods Eng 1970;2(2):229–41.
[30] Wriggers P. Nonlinear finite element methods. Berlin: Springer; 2008.
[31] Challamel N, Wang CM, Elishakoff I. Discrete systems behave as nonlocal structural elements: bending, buckling and vibration analysis. Eur. J. Mech. A/Solids 2014;44:125–35.